

PAPER • OPEN ACCESS


## Generation and characterization of polarization-entangled states using quantum dot single-photon sources

To cite this article: Mauro Valeri *et al* 2024 *Quantum Sci. Technol.* **9** 025002

View the [article online](#) for updates and enhancements.

You may also like

- [CEWQO Topical Issue](#)  
Mirjana Bozic and Margarita Man'ko
- [How to control decoherence and entanglement in quantum complex systems?](#)  
V M Akulin, G Kurizki and D A Lidar
- [Effect of depolarizing noise on entangled photons](#)  
Ruchipas Bavontaweepanya

 **kiutra**

Easy-to-use and Helium-3 free  
cryogenics solutions

LEARN MORE

# Quantum Science and Technology



## PAPER

### OPEN ACCESS

RECEIVED  
9 August 2023

REVISED  
13 December 2023

ACCEPTED FOR PUBLICATION  
8 January 2024

PUBLISHED  
22 January 2024

Original Content from  
this work may be used  
under the terms of the  
[Creative Commons  
Attribution 4.0 licence](#).

Any further distribution  
of this work must  
maintain attribution to  
the author(s) and the title  
of the work, journal  
citation and DOI.



## Generation and characterization of polarization-entangled states using quantum dot single-photon sources

Mauro Valeri , Paolo Barigelli , Beatrice Polacchi , Giovanni Rodari , Gianluca De Santis, Taira Giordani , Gonzalo Carvacho\* , Nicolò Spagnolo and Fabio Sciarrino

Dipartimento di Fisica, Sapienza Università di Roma, Piazzale Aldo Moro 5, I-00185 Roma, Italy

\* Author to whom any correspondence should be addressed.

E-mail: [gonzalo.carvacho@uniroma1.it](mailto:gonzalo.carvacho@uniroma1.it)

**Keywords:** entangled photon sources, quantum information, quantum optics, quantum dots

Supplementary material for this article is available [online](#)

### Abstract

Single-photon sources based on semiconductor quantum dots find several applications in quantum information processing due to their high single-photon indistinguishability, on-demand generation, and low multiphoton emission. In this context, the generation of entangled photons represents a challenging task with a possible solution relying on the interference in probabilistic gates of identical photons emitted at different pulses from the same source. In this work, we implement this approach via a simple and compact design that generates entangled photon pairs in the polarization degree of freedom. We operate the proposed platform with single photons produced through two different pumping schemes, the resonant excited one and the longitudinal-acoustic phonon-assisted configuration. We then characterize the produced entangled two-photon states by developing a complete model taking into account relevant experimental parameters, such as the second-order correlation function, Hong–Ou–Mandel visibility, multiphoton emission and pump laser filtering. Our source shows long-term stability and high quality of the generated entangled states, thus constituting a reliable building block for optical quantum technologies.

## 1. Introduction

The generation of entangled states of light is fundamental to several quantum information applications ranging from quantum communication [1–3], quantum sensing and metrology [4, 5], quantum networks [6–9] and quantum computing [10–12]. Spontaneous parametric down-conversion-based sources can be employed to obtain high-fidelity entangled photons. However, this technology presents a trade-off between the brightness and quality of the output states. Indeed, due to the probabilistic nature of the process, increasing source brightness is inherently accompanied by higher multiphoton terms, and thus the generation rate must be kept below a certain threshold; such limitation can be overcome by exploiting quantum dot (QD) sources [13, 14]. In the last 20 years, QD single-photon sources (SPSs) have been widely exploited for secure quantum communication [15, 16] due to their simultaneous characteristics of high purity, brightness and single-photon indistinguishability. Moreover, QD-based SPSs represent a favorable approach for measured-based quantum computing [17], optical quantum networks [7], generation of photonic cluster states [18] and high-performance boson sampling [19]. In particular, it has been recently demonstrated that SPSs provide a significant improvement in quantum key distribution (QKD) schemes due to their low multi-photon contribution, thus minimizing information leakage to malicious eavesdroppers [20]. For this reason, QD sources have been mainly adopted in standard BB84 protocols [15, 21, 22], representing a natural solution to multiphoton-based attack as well as QKD protocols based on entangled photon sources (EPSs) [3, 23, 24]. Furthermore, QD-based SPSs (QDSPs) are being also exploited for the generation of Greenberger–Horne–Zeilinger (GHZ) states using integrated photonics [25] thus demonstrating their successful application in multipartite protocols [26, 27].

Entanglement generation by means of QDSPs has been investigated by employing different degrees of freedom and configurations, such as structured photons [28], polarization-encoded GHZ states based on temporal-delay fiber loops [29–31], spin-photon entanglement [32, 33], and time-distributed photon-number entangled states [34]. Designing QDs without fine structure splitting (FSS) that generates a pair of entangled photons via biexciton–exciton radiative cascade [23, 35, 36] represents one of the most common applications and efficient methods. However, the quality of the entangled states is degraded when FSS is present. Therefore, the development of alternative schemes to generate entanglement for this case is pivotal for further extending the study of QD-based protocols. Nowadays, the generation of entangled states exploiting non-entangled emission by QDs has been demonstrated in a few works [29, 30, 37, 38] and represents a practical possibility to scale QD-based GHZ states [30]. Nevertheless, a complete model accounting for the QD source properties as well as other sources of experimental imperfections, such as residual pump laser, multiphoton emission and overall efficiency of the experimental setup is still lacking. Filling this gap is necessary to fully determine important properties such as entanglement and stability, whose characterization is fundamental for protocols such as QKD. The single-photon emission by exciton-based QD can be achieved in two different regimes, the first one with the pumping laser being resonant with the exciton energy level and the non-resonant excitation [14]. On one hand, the main advantage of non-resonant excitation resides in the fact that single photons emitted can be easily separated from the excitation laser through spectral filtering. On the other hand, resonant fluorescence (RF) can be adopted to improve single-photon indistinguishability, eliminating dephasing and time jitter [39], at the price of more challenging suppression of the residual pump laser light. Also, due to the cross-polarization filtering procedure of the residual pump, the Firs lens brightness is at least halved [13].

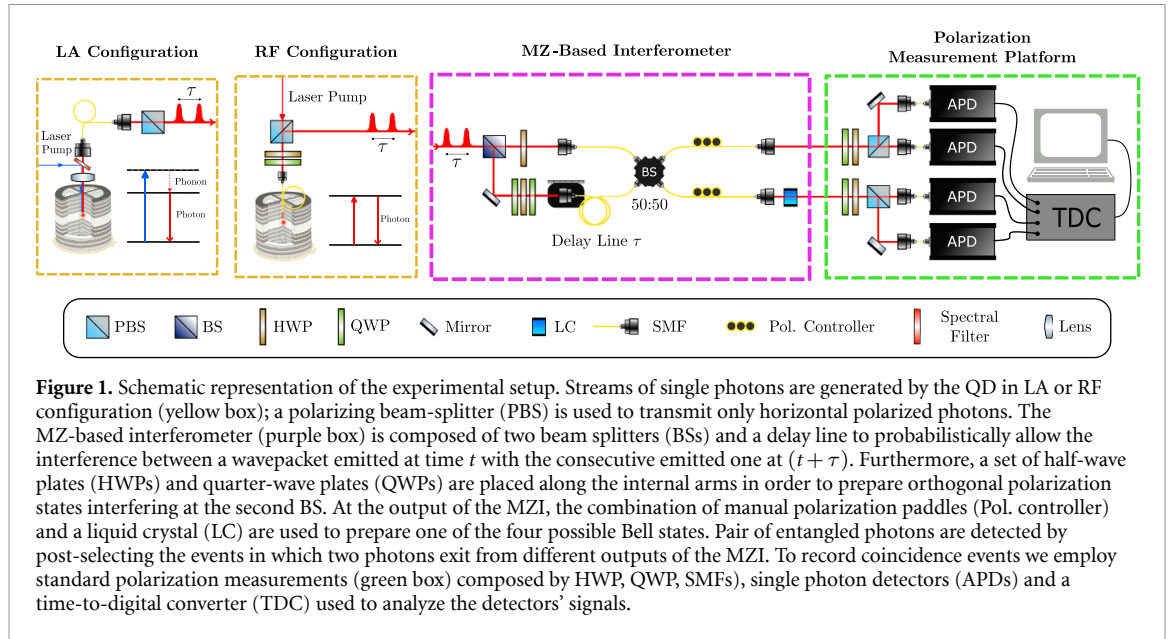
In this work, we design and fully characterize an optical scheme to generate polarization-entangled pairs of photons using a semiconductor QD device emitting highly indistinguishable single-photon streams. Two QDs were considered for the study: one coherently controlled via RF excitation, and the other operated under non-resonant excitation assisted by longitudinal-acoustic (LA) phonons [14]. In our design, the entangled pairs are obtained by employing interference between two photons generated in two consecutive pulses by the QD source, and, therefore, the overall quality of the generated states depends on the indistinguishability of the exploited photons. This feature has been extensively discussed in terms of Hong–Ou–Mandel (HOM) effect and multiphoton contributions [40]. The resulting performance of the polarization-entangled source is quantified by directly measuring the brightness and through a CHSH test [41] for both QD excitation schemes.

Finally, to determine the quality of the entanglement that can be generated, we present a model involving several experimental parameters of our system. We tested the time-stability and the robustness of the generated entangled states while these parameters varied. In this way, we identified the quantities which mainly affect the quality of the generated entangled state, i.e. the degree of indistinguishability between consecutive emissions and the multi-photon component of the QD source itself.

## 2. Experimental platform

The experimental platform is depicted in figure 1. Both QDSPs are commercial Quandela *e-Delight* systems (yellow dotted line panel). The semiconductor devices consist of a InGaAs matrix placed in a nanoscale electrically controlled micropillar cavity [42] kept at cryogenic temperature (around 4 K) by an *Attocube-Attodry800* He-closed cycle cryostat. The QDSPs are optically excited by a 79 MHz-pulsed laser in two different excitation schemes: the first device works in a longitudinal phonon-assisted configuration (LA) [43], while emission for the second device is achieved resonantly in the so-called RF one [44].

The LA optical excitation (QD<sup>LA</sup>) is obtained by blue-detuning the laser pump at 927.2 nm, and produces single photons at 927.8 nm. The emitted photons are coupled into a single-mode fibers (SMF) through a free-space confocal microscope mounted atop of the cryostat shroud and spectrally separated from the residual pumping laser with spectral filters. The RF optical excitation (QD<sup>RF</sup>) employs a laser pump at a wavelength centered at 928.05 nm, enabling resonant single photon generation by exciton emission. For this second QDSP, we achieve the single photon collection by means of an SMF located almost in direct contact with the sample inside the cryostat. Photons are separated from the residual pumping laser in a cross-polarization configuration. The train of single photons is sent to an unbalanced Mach–Zehnder-based interferometer (MZI) for the generation of entangled photon pairs in the polarization degree of freedom (purple dotted line panel in figure 1). A first in-bulk balanced beam splitter (BS) divides the photons into two paths, with a relative temporal delay corresponding to the difference between two consecutive emissions (~12 ns) achieved through a specifically tuned fiber delay line. A photon entering the shorter path is



prepared in vertical polarization (V), while the photon in the longer path is prepared in horizontal polarization (H). A second in-fiber 50/50 BS recombines the two signals. In this way, when two consecutive photons—namely head and tail—take different internal paths of the MZI, if the tail photon takes the shorter path it then recombines in the BS with the head one. Precise temporal overlap between the photon pairs, on the output BS, is achieved by finely adjusting the delay line along the longer path. Finally, when post-selecting on the cases when photons take different output paths, i.e. on two-fold coincidences, the obtained theoretical output state is  $|\psi^{(\phi)}\rangle = \frac{1}{\sqrt{2}}(|HV\rangle + e^{i\phi}|VH\rangle)$ . A liquid crystal (LC) sets the phase  $\phi$ , while polarization controllers are used to prepare one of the four states of the Bell basis. The measured coincidence rate exiting the MZI is  $R_{CC}^{\text{measured}} = 1 \text{ kHz}$  (0.5 kHz) for  $QD^{\text{LA}}$  ( $QD^{\text{RF}}$ ). This value is compatible with the transmission efficiency of the apparatus (50%). Indeed, considering a near-unity generation rate inside the QD cavity ( $R_{QD} \sim 79 \text{ MHz}$ ), the probability of detecting a zero-delay coincidence at the output of the MZI is first reduced by a factor 4 from the first BS—i.e. the success probability of obtaining the head photon in the delayed path and the tail photon in the shorter path of the MZI—and then halved by the post-selection process, thus providing a final expected coincidence rate:  $R_{CC} = \frac{\eta_{\text{tot}}^2}{8} R_{QD}$ , where  $\eta_{\text{tot}}$  is the total transmission of the experimental platform (see the supplementary information for a detailed description of the loss budget). The quality of the generated entangled state mainly depends on the indistinguishability of consecutively emitted photons as well as the presence of multi-photon components. These characteristics can be quantified and studied, respectively, through the visibility  $V_{\text{HOM}}$  of the HOM effect, and the second-order correlation function  $g^{(2)}(0)$ .

### 3. Results

#### 3.1. Theoretical model

When realizing an experimental platform for the generation of entangled states we necessarily have to take into account multiple factors that preclude the realization of an ideal maximally entangled pure state. In what follows, we describe a model which identifies the main parameters of our experimental apparatus and relate them to the quality of the output entangled state. A detailed investigation of such quantities is reported in the supplementary information.

The first parameter to be considered is the degree of indistinguishability between the two interfering photons generating the entangled state, which depends on the overlap of their wavepackets. This overlap is commonly quantified by measuring the visibility of HOM effect. Indeed, when two partially distinguishable photons impinge on the inputs of a balanced BS there is a non-zero probability  $P_{cc}$  of obtaining a coincidence event at the two outputs of the BS, which is at most equal to  $P_{cc} = 1/2$  for fully distinguishable photons. The measured HOM visibility  $V_{\text{HOM}}$  is then quantified as:

$$V_{\text{HOM}} = 1 - 2P_{cc}. \quad (1)$$

This quantity is equal to one for perfectly indistinguishable photons, that is, no coincidence counts are detected at the output of the BS; this is the typical signature of the HOM effect. However, the experimentally measured HOM visibility ( $V_{\text{HOM}}$ ) does not match with the true photon indistinguishability ( $V$ ), namely the single photon trace purity [40]. This is due to the possible presence of additional photons (defined as noise photons) traveling together with the SPS signal. Despite the QDs employed in the experiment show a high probability  $p_1$  of single-photon generation for each pump pulse ( $p_1 \sim 1$  for resonant excitation,  $p_1 \leq 1$  for phonon-assisted excitation [43]), a residual probability  $p_2$  of noise-photon component exists, such that  $p_0 + p_1 + p_2 = 1$ , where  $p_0$  is the probability of no-excitation. The generated state in the LA configuration is a statistical mixture of vacuum state and one-photon state while in the RF regime, the general description of emitted photon state is given by a vacuum-one photon coherent superposition state, i.e.  $\sqrt{1-q}e^{i\phi_q}|0\rangle + \sqrt{q}|1\rangle$  with  $q \in [0, 1]$ ,  $\phi_q \in \mathbb{R}$ , where the parameter  $q$  can in principle be varied by tuning the laser pump intensity and ideally is set to near unity [44]. To quantify the impact of noisy photons, a measurement of the second-order correlation  $g^{(2)}(0)$  can be performed through the Hanbury–Brown–Twiss (HBT) setup. The probability of having more than one photon  $p_2$  is then computed through the relation  $g^{(2)}(0) = \frac{2p_2}{(p_1+2p_2)^2}$ , as detailed in supplementary note 1. Furthermore, the measured HOM visibility  $V_{\text{HOM}}$  is reduced if the employed BS is not perfectly symmetric, that is, with reflectivity  $R = 1/2$ . In particular, according to [40], the relation between multiphoton emission and photon indistinguishability is given by:

$$V_{\text{HOM}} = 4RT \left( 1 + V - \frac{1+V}{1-v_{\text{sn}}} g^{(2)}(0) \right) - 1, \quad (2)$$

where  $T$  ( $R$ ) is the transmissivity (reflectivity) of the BS and  $v_{\text{sn}}$  is the overlap between the single photon signal and the noise photons. Therefore, considering the additional photon distinguishable from the QD signal, i.e.  $v_{\text{sn}} = 0$  and a 50:50 BS, it is possible to compute a more precise estimation of the photon indistinguishability as:

$$V = \frac{V_{\text{HOM}} + g^{(2)}(0)}{1 - g^{(2)}(0)}. \quad (3)$$

The partial indistinguishability and the use of non-ideal BSs in the interferometer cause the state produced by the two-photon interference ( $\hat{\rho}_{11}$ ) to be different from the ideal pure state ( $\hat{\rho}_{\psi} = |\psi^{(\phi)}\rangle\langle\psi^{(\phi)}|$ ), that is  $\hat{\rho}_{11} \neq \hat{\rho}_{\psi}$ . In particular, the distinguishability among the photons has different origins and its effect on the final state of the source is to introduce non-ideal terms, that acts as dephasing and white noise. Indeed, the presence of noise photons not only changes the estimation of HOM visibility, but also provides a contribution to the final state, that we indicate as  $\hat{\rho}_{12}$ ,  $\hat{\rho}_{02}$  and  $\hat{\rho}_I$  (equation (2) of supplementary information). Such multi-photon component gives rise to noise terms such as  $|HH\rangle\langle HH|$  and  $|VV\rangle\langle VV|$ , as well as to terms  $|HV\rangle\langle HV|$  and  $|VH\rangle\langle VH|$  in the final state. The probability of each term depends on the generation mechanism, described in detail in the supplementary information. Furthermore, to take into account optical components imperfections or any other constant noise, like darkcounts, a contribution of white noise  $\hat{\rho}_{\text{wn}} = \mathbb{I}/4$  is added to the experimental state since these terms provide a uniform contribution to the coincidence counts in all the bases. The weight of the uniform contribution with respect to the experimental state is determined by the coefficient  $c_{\text{wn}}$ . Therefore, the expected experimental state has the form:

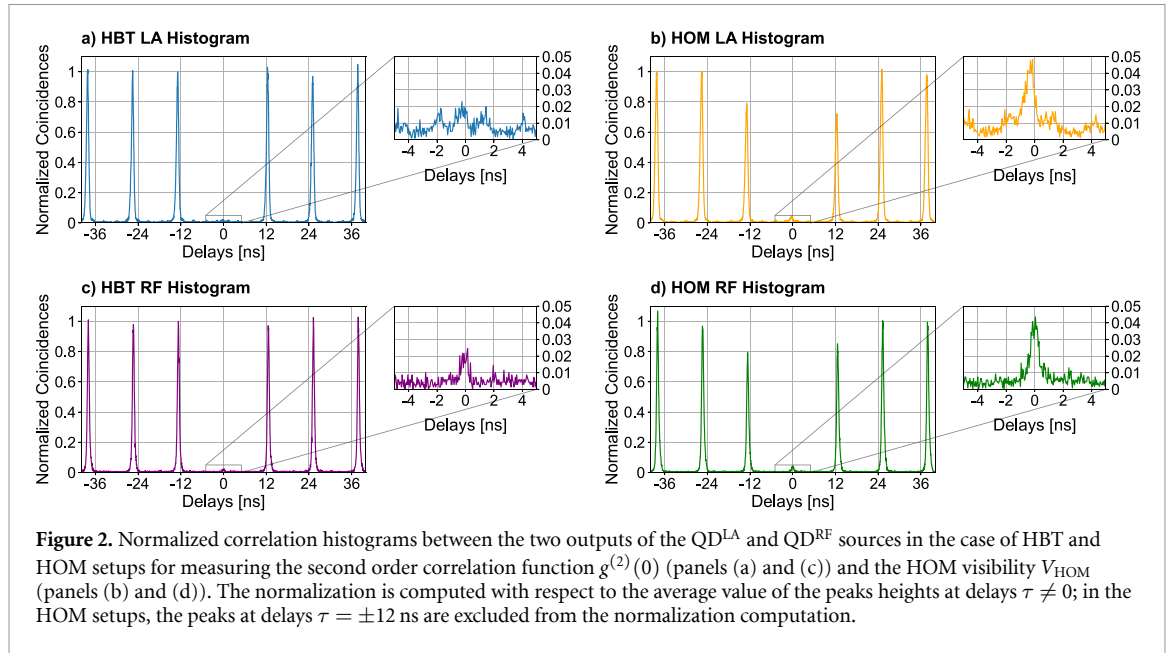
$$\hat{\rho} = c_{\text{wn}}\hat{\rho}_{\text{exp}} + (1 - c_{\text{wn}}) \frac{\mathbb{I}}{4} \quad (4)$$

where

$$\hat{\rho}_{\text{exp}} = c_{11}\hat{\rho}_{11} + c_{12}\hat{\rho}_{12} + c_{02}\hat{\rho}_{02} + c_I\hat{\rho}_I. \quad (5)$$

The coefficients  $c_{02}$ ,  $c_{11}$ ,  $c_{12}$ ,  $c_I$  depend on several parameters such as the overall transmissivity  $\eta$  and the percentage of a multi-photon signal expressed through the probability  $p_0$ ,  $p_1$ ,  $p_2$  to have zero, one and two photons emission respectively (see supplementary information). The explicit expressions of the matrices  $\hat{\rho}_{11}$ ,  $\hat{\rho}_{12}$ ,  $\hat{\rho}_{02}$ , and  $\hat{\rho}_I$  are reported in the supplementary information.

Using equation (4), it is possible to compute the maximum degree of entanglement achievable with our experimental setup. Furthermore, the quality of the entanglement can be asserted in a device-independent manner by using a Bell-CHSH test [41]. According to its formulation, the presence of entanglement between two subsystems (A and B) is a necessary condition to violate the classical bound of the Bell-CHSH inequality:



$$S = |E(A_0, B_0) + E(A_0, B_1) + E(A_1, B_0) - E(A_1, B_1)| \leq 2 \quad (6)$$

where  $E(A_i, B_j)$  (with  $i, j = 0, 1$ ) is the expectation value of the correlator between two possible dichotomic measurements made locally on the subsystems A and B. It is well known that maximally entangled states, like the Bell states, can reach  $S = 2\sqrt{2}$  which is the maximal violation of the Bell-CHSH inequality allowed within quantum mechanics. For simplicity, we consider the so-called singlet Bell state ( $\phi = \pi$ , so that  $|\psi^{(\phi)}\rangle = |\psi^{(-)}\rangle$ ). To achieve  $S = 2\sqrt{2}$  with a singlet state, one can choose as measurements  $\hat{A}_0 = \hat{\sigma}_z$ ,  $\hat{A}_1 = \hat{\sigma}_x$  and  $\hat{B}_0 = (\hat{\sigma}_z + \hat{\sigma}_x)/\sqrt{2}$ ,  $\hat{B}_1 = (\hat{\sigma}_z - \hat{\sigma}_x)/\sqrt{2}$ , where  $\hat{\sigma}_z$  and  $\hat{\sigma}_x$  are the standard Pauli operators.

The state in equation (4) corresponds to a lower violation of the Bell inequality with respect to its maximum value of  $2\sqrt{2}$  achievable via a singlet state. Here the expectation values of the correlators over the modeled state have been computed as  $E(A_i, B_j) = \text{Tr}[\hat{\rho}_{\text{exp}} \hat{A}_i \otimes \hat{B}_j]$  with  $i, j = 0, 1$ . As a result this relation shows the strongest dependence on the parameters  $g^{(2)}(0)$  and  $c_{\text{wn}}$ , i.e. the fraction of white noise. Conversely, the highest achievable value of  $S$  does not depend significantly from non-ideal splitting ratios of the BSs.

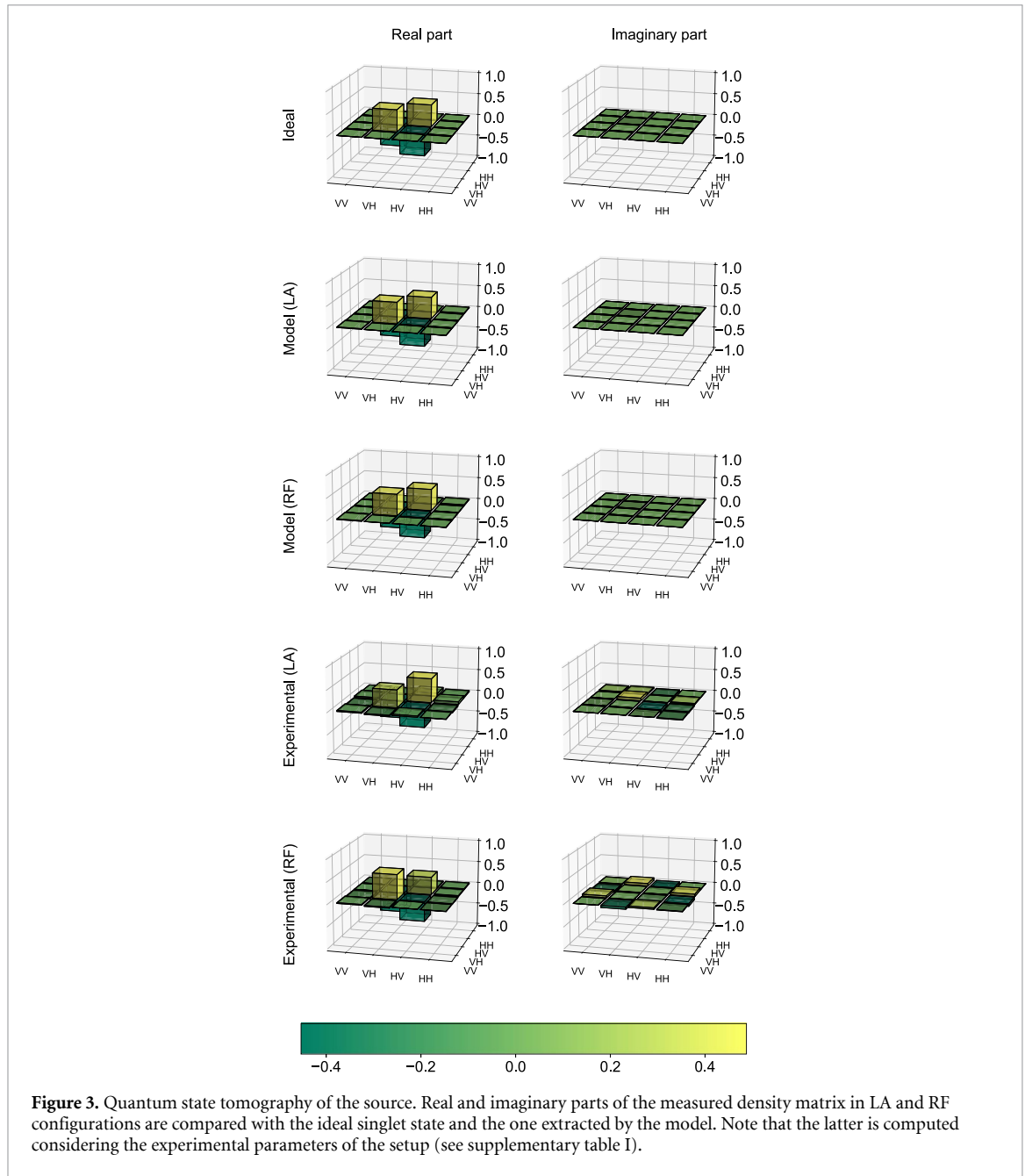
Similar results hold when considering the fidelity  $\mathcal{F}$  with respect to the ideal singlet state  $\hat{\rho}_{\psi^{(-)}}$ , defined as:

$$\mathcal{F} = \text{Tr} \left[ \sqrt{\sqrt{\hat{\rho}_{\psi^{(-)}}} \hat{\rho} \sqrt{\hat{\rho}_{\psi^{(-)}}}} \right]^2. \quad (7)$$

In the supplementary information we describe a complete model of the main parameters affecting the maximum achievable Bell-CHSH violation  $S$  and fidelity  $\mathcal{F}$  over the experimentally generated state  $\hat{\rho}$ . Since the RF configuration operates in the regime  $q \sim 1$ , the differences between the RF and LA models reside in the computation of the probabilities  $p_1$  and  $p_2$ , quantified by the  $g^{(2)}(0)$ . Moreover, we note that there is no difference in the entanglement quality obtained via the two different excitation schemes when the RF source is operated in the near  $\pi$ -pulse regime.

### 3.2. Performances

The measured two-photon coincidence rate at the output of the source is  $R_m^{\text{LA}} = 1$  kHz ( $R_m^{\text{RF}} = 0.5$  kHz). The single photon detectors used have a detection efficiency of around  $\eta_d \sim 35\%$ , from which it is possible to infer the generated rate by the source of  $R_g^{\text{LA}} \sim 8$  kHz ( $R_g^{\text{RF}} \sim 4$  kHz). Such rate can be improved by a factor 4 replacing the passive demultiplexer, i.e. the first BS of the MZI, with deterministic choice of the path for the consecutive photons, sending deterministically the head (tail) photon in the longer (shorter) path. This active demultiplexing can be realized, for example, by adopting an electro-optic modulator and a polarizing BS (PBS) [45]. As explained previously, the quality of the produced state is evaluated in terms of  $g^{(2)}(0)$  and the indistinguishability of consecutive photons. The former is computed with an HBT setup—obtained by blocking one arm of the interferometer—while the latter by using the half-wave plates to rotate the photon polarization in the shorter path from vertical to horizontal (the same as the photon in the longer path). Figure 2 shows the time correlation histograms for both measures: QD<sup>LA</sup> provides  $V_{\text{HOM}}^{\text{LA}} = (90.3 \pm 0.3)\%$

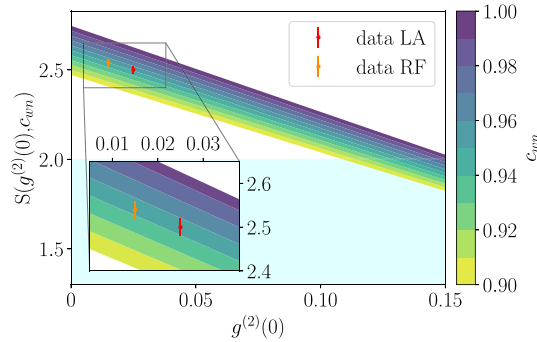


**Figure 3.** Quantum state tomography of the source. Real and imaginary parts of the measured density matrix in LA and RF configurations are compared with the ideal singlet state and the one extracted by the model. Note that the latter is computed considering the experimental parameters of the setup (see supplementary table I).

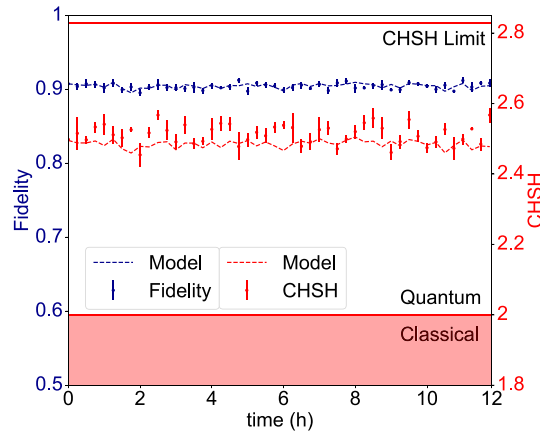
and  $g_{LA}^{(2)}(0) = (1.2 \pm 0.1)\%$ , while for  $QD^{RF}$  the measured values are  $V_{HOM}^{RF} = (91.8 \pm 0.2)\%$  and  $g_{RF}^{(2)}(0) = (1.6 \pm 0.2)\%$ . According to equation (3), the HOM visibility corrected by  $g^{(2)}(0)$  are found to be  $V^{LA} = (92.7 \pm 0.3)\%$  and  $V^{RF} = (94.9 \pm 0.3)\%$ . Polarization measurement stages are placed at the two outputs of the MZI in order to characterize in detail the final state of the source. After fine-tuning of the LC for setting the singlet Bell state, a quantum state tomography and the CHSH test have been made. The resulting density matrix is shown in figure 3, which correspond to a fidelity  $\mathcal{F}_{raw}^{LA} = (90 \pm 1)\%$  and  $\mathcal{F}_{raw}^{RF} = (92 \pm 1)\%$  with respect to the ideal singlet state  $\hat{\rho}_{\psi^{(-)}}$ . Considering the accidental counts measured in the middle of two pulses of the time-correlation histogram (e.g. at delay 6 ns), it is possible to extract only the noise contribution due to detector dark counts which affect such fidelities. By subtracting this contribution, we obtain a fidelity of  $\mathcal{F}^{LA} = (92 \pm 1)\%$  and  $\mathcal{F}^{RF} = (95 \pm 1)\%$ . As previously discussed, non-ideal contributions that limit the fidelity derive from multi-photon components, white noise and actual distinguishability of single photons emitted by the QD sources, according to equation (4). Finally, we measured the CHSH parameter obtaining  $S_{raw}^{LA} = (2.50 \pm 0.02)$  from raw data, and  $S^{LA} = (2.58 \pm 0.02)$  subtracting dark counts in the case of  $QD^{LA}$ . Similarly, the use of  $QD^{RF}$  provides  $S_{raw}^{RF} = (2.54 \pm 0.02)$  and  $S^{RF} = (2.63 \pm 0.02)$ . Table 1 shows the performances of the two different configurations. The effect of  $g^{(2)}(0)$  and  $V$  on the S maximum values achievable can be quantified from the theoretical model via the

**Table 1.** Comparison of the maximum experimental values measured between the (LA) and (RF) configurations.

	LA	RF
$\eta$	0.83%	0.51%
$g^{(2)}(0)$	$(1.2 \pm 0.1)\%$	$(1.6 \pm 0.2)\%$
$V$	$(92.7 \pm 0.3)\%$	$(94.9 \pm 0.3)\%$
$\mathcal{F}$	$(92 \pm 1)\%$	$(95 \pm 1)\%$
$S$	$2.58 \pm 0.02$	$2.63 \pm 0.02$



**Figure 4.** Maximum achievable value of the Bell-CHSH quantity as a function of the  $g^{(2)}(0)$  and the fraction of white noise due to state polarization imperfection and darkcounts ( $c_{\text{wn}}$ ). The experimental points are  $(0.025 \pm 0.002, 2.50 \pm 0.02)$  for LA (red) and  $(0.015 \pm 0.002, 2.54 \pm 0.02)$  for RF (orange) without subtracting accidental coincidences which are compatible with  $c_{\text{wn}} \sim 0.95$ . For simplicity, RF and LA data have been plotted together due to the very low difference in the theoretical model predicting the expectation values of  $S_{\text{raw}}$ .

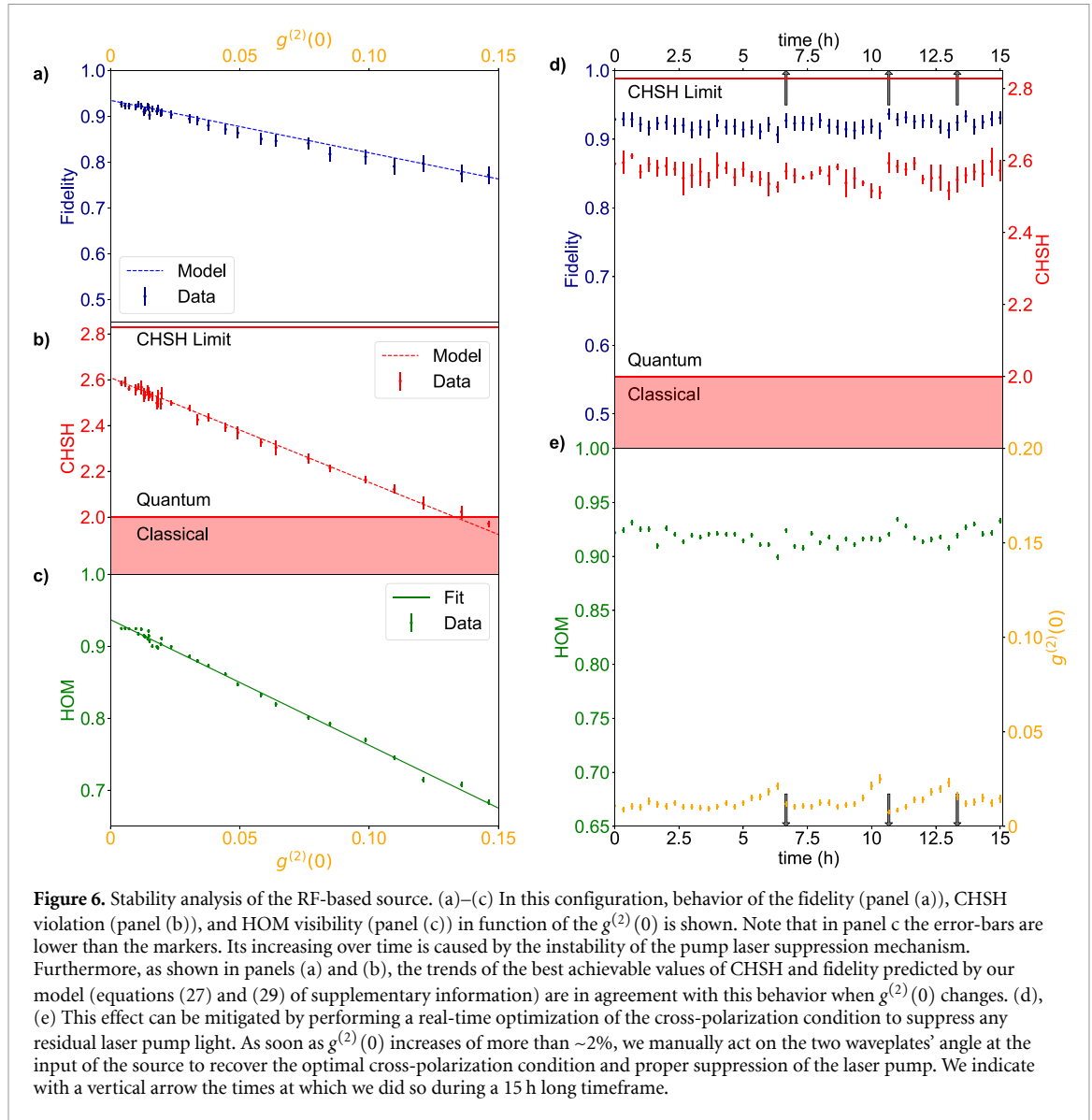


**Figure 5.** Performances of the LA-based source as a function of the time. Long-term stability of the source is monitored in terms of fidelity (left vertical axis) and CHSH violation (right vertical axis) during 12 h of operation. The dotted lines correspond to the theoretical prediction with  $c_{\text{wn}} = 0.95$ . Note that classical/quantum regions are referred to the Bell's parameter while the solid red lines stands for the minimum/maximum value of the CHSH parameter.

ratio of the partial derivative around the point  $g^{(2)}(0) \rightarrow 0$ ,  $V = 1$ . The ratio corresponds to  $\sim 8.5$  in favor of  $g^{(2)}(0)$ , showing that  $S$  is more sensitive with respect to variation of the photon overlap. Repeating the reasoning for the fidelity, the same ratio is  $\sim 2.5$  in both configurations. In figure 4 we compare the measured values of  $S_{\text{raw}}^{\text{LA}}$  and  $S_{\text{raw}}^{\text{RF}}$  with the expected values of the CHSH parameter according to the proposed model (see supplementary information). The plot shows how the second-order correlation function reduces the maximum achievable  $S$  by our experimental scheme; it also predicts the maximum value of  $S$  obtainable given the value of  $g^{(2)}(0)$  and  $c_{\text{wn}}$ . As expected, the observed experimental values do not exceed the maximum values predicted by the model.

Figure 5 shows the stability of the produced quantum state in time, demonstrating no drop in performance over 12 h without user intervention in the case of longitudinal phonon-assisted excitation. Such a feature is relevant when the source is used for long duration measurement protocols. Conversely, the RF approach showed less stability, having a drop in performance after few hours (figures 6(d) and (e)). As shown by the figures 6(a)–(c) this reduced stability is related to an increasing  $g^{(2)}(0)$  while the variation of





other parameters have reduced or no effects. According to [40], a linear fit made with the parameters  $V_{\text{HOM}}$  and  $g^{(2)}(0)$  returns the value of the photon superposition equal to  $V = 0.937 \pm 0.001$ . The predictions of the theoretical model are compatible with the experimental data considering a uniform noise quantified by  $c_{\text{wn}} \sim 0.95$ . The increasing  $g^{(2)}(0)$  is related to the non-perfect elimination of the pump laser by the polarization-based suppression system. In fact, figures 6(d) and (e) show how the performance was recovered by resetting that suppression whenever it showed a decrease.

#### 4. Conclusions

We demonstrated a simple design to generate pairs of entangled photons in polarization by employing a QD device emitting single photons streams. Our source is based on a MZI-like configuration, having long-term stability and providing high quality of the entangled pair. Its characterization in both LA and RF configurations demonstrated a high fidelity of the produced state with respect to the ideal single Bell state, i.e.  $\mathcal{F}_{\text{raw}}^{\text{LA}} = (90 \pm 1)\%$  and  $\mathcal{F}_{\text{raw}}^{\text{RF}} = (92 \pm 1)\%$ , and certified the presence of non-locality by violating CHSH inequality achieving  $S_{\text{raw}}^{\text{LA}} = (2.50 \pm 0.02)$  and  $S_{\text{raw}}^{\text{RF}} = (2.54 \pm 0.02)$ , respectively. Entangled-based quantum communication protocols using QD have so far been demonstrated only with EPSs [23]. The performances of our source enable such implementations also adopting QDSPS as well. In fact, despite the presence of post-selection on coincidence events, the security of QKD protocols is not further affected because the same post-selection procedure is repeated on the algorithms based on entangled states [24]. With respect to previous works, the most innovative aspect of this manuscript is two-fold. On one hand, we employ both a resonant and an off-resonant excitation scheme for our QD sources, as well as two different configurations

for laser injection and photon extraction, showing the entanglement generation and stability performances of both schemes by measuring the same figures of merit over more than 10 h. On the other, we provide a precise and accurate theoretical model to predict and directly test the quality of the entangled state that takes into account noise sources that have not been taken into consideration in previous works. Our results found particular relevance in protocols sensitive to these experimental parameters, such as QKD, where multiphoton emission as well as pump filtering play a key role. Therefore, this work represents a significant step forward in the generation of entanglement states via QDSPS exciton emission. Indeed, similar source-designs have been considered for such purposes [29, 30]. The results demonstrate that the main factors limiting our source are  $g^{(2)}(0)$ , HOM visibility and white noise. In presence of high indistinguishability and low multiphoton emission, our design shows great stability in generating high quality entangled photon pairs in polarization, despite possible non-idealities of the parameters which constitute the source structure (e.g. splitting ratio of BSs) or long-time measurements. We stress that, by improving the filtering system for the LA configuration or by adopting accurate feedback mechanisms to control the cross-polarization condition in the RF configuration, a value closer to the intrinsic  $g^{(2)}(0)$  of the source can be achieved, thus increasing, in turn, the value of fidelity and the Bell's inequality violation. Moreover, our scheme constitutes a modular and versatile plug-in architecture that can be easily tailored to several types of SPSs and unplugged whenever independent single photons are needed. Thus, the measured CHSH values together with the tomography process, confirm the high purity of the employed QD device in emitting highly indistinguishable single photons. Our setup can be exploited for the generation of entangled photons to be used in several quantum information protocols, as those using integrated photonics for fundamental tests [46–48], boson sampling [49–51] and hybrid entanglement between different degrees of freedom such as orbital angular momentum-polarization [28, 52, 53], to cite some examples.






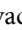

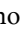
### Data availability statement

All data that support the findings of this study are included within the article (and any supplementary files).

### Acknowledgments

We thank Petr Stepanov, Niccolo Somaschi and *Quandela* for all the support provided. This work is supported by the ERC Advanced Grant QU-BOSS (Grant Agreement No. 884676) and by the PNRR MUR Project PE0000023-NQSTI.

### ORCID iDs

Mauro Valeri  <https://orcid.org/0000-0003-1094-6839>  
Paolo Barigelli  <https://orcid.org/0009-0006-9402-7571>  
Beatrice Polacchi  <https://orcid.org/0000-0003-3133-3564>  
Giovanni Rodari  <https://orcid.org/0000-0002-6056-4583>  
Taira Giordani  <https://orcid.org/0000-0001-7111-0272>  
Gonzalo Carvacho  <https://orcid.org/0000-0003-4465-3401>  
Nicolò Spagnolo  <https://orcid.org/0000-0003-3471-2252>  
Fabio Sciarrino  <https://orcid.org/0000-0003-1715-245X>

### References

- [1] Vajner D A, Rickert L, Gao T, Kaymazlar K and Heindel T 2022 *Adv. Quantum Technol.* **5** 2100116
- [2] Ma X, Fung C-H F and Lo H-K 2007 *Phys. Rev. A* **76** 012307
- [3] Schimpf C, Reindl M, Huber D, Lehner B, da Silva S F C, Manna S, Vvylecka M, Walther P and Rastelli A 2021 *Sci. Adv.* **7** eabe8905
- [4] Giovannetti V, Lloyd S and Maccone L 2011 *Nat. Photon.* **5** 222
- [5] Huang Z, Macchiavello C and Maccone L 2016 *Phys. Rev. A* **94** 012101
- [6] Carvacho G et al 2022 *Optica* **9** 572
- [7] Lu C-Y and Pan J-W 2021 *Nat. Nanotechnol.* **16** 1294
- [8] Lodahl P 2017 *Quantum Sci. Technol.* **3** 013001
- [9] Li B, Li Y-H, Cao Y, Yin J and Peng C-Z 2023 *Phys. Rev. Appl.* **19** 064083
- [10] DiVincenzo D P 1995 *Science* **270** 255
- [11] O'Brien J L 2007 *Science* **318** 1567
- [12] Loss D and DiVincenzo D P 1998 *Phys. Rev. A* **57** 120
- [13] Wang H et al 2019 *Nat. Photon.* **13** 770
- [14] Senellart P, Solomon G and White A 2017 *Nat. Nanotechnol.* **12** 1026
- [15] Waks E, Inoue K, Santori C, Fattal D, Vuckovic J, Solomon G S and Yamamoto Y 2002 *Nature* **420** 762
- [16] Bozzio M, Vvylecka M, Cosacchi M, Nawrath C, Seidelmann T, Loredo J C, Portalupi S L, Axt V M, Michler P and Walther P 2022 *npj Quantum Inf.* **8** 104

- [17] Zwerger M, Briegel H and Dür W 2016 *Appl. Phys. B* **122** 50
- [18] Lindner N H and Rudolph T 2009 *Phys. Rev. Lett.* **103** 113602
- [19] Wang H et al 2017 *Nat. Photon.* **11** 361
- [20] Brassard G, Lütkenhaus N, Mor T and Sanders B C 2000 *Phys. Rev. Lett.* **85** 1330
- [21] Rau M et al 2014 *New J. Phys.* **16** 043003
- [22] Takemoto K, Nambu Y, Miyazawa T, Sakuma Y, Yamamoto T, Yorozu S and Arakawa Y 2015 *Sci. Rep.* **5** 1
- [23] Basso Basset F et al 2021 *Sci. Adv.* **7** eabe6379
- [24] Basso Basset F et al 2022 *Quantum Sci. Technol.* **8** 025002
- [25] Pont M et al 2022 High-fidelity generation of four-photon GHZ states on-chip (arXiv:2211.15626 [quant-ph])
- [26] Hillery M, Bužek V and Berthiaume A 1999 *Phys. Rev. A* **59** 1829
- [27] Proietti M, Ho J, Grasselli F, Barrow P, Malik M and Fedrizzi A 2021 *Sci. Adv.* **7** eabe0395
- [28] Suprano A et al 2023 *Adv. Photonics* **5** 046008
- [29] Istrati D et al 2020 *Nat. Commun.* **11** 1
- [30] Li J-P, Qin J, Chen A, Duan Z-C, Yu Y, Huo Y, Höfiling S, Lu C-Y, Chen K and Pan J-W 2020 *ACS Photonics* **7** 1603
- [31] Cogan D, Su Z-E, Kenneth O and Gershoni D 2023 *Nat. Photon.* **17** 324
- [32] De Greve K et al 2012 *Nature* **491** 421
- [33] Schwartz I, Cogan D, Schmidgall E R, Don Y, Gantz L, Kenneth O, Lindner N H and Gershoni D 2016 *Science* **354** 434
- [34] Wein S C et al 2022 *Nat. Photon.* **16** 374
- [35] Wang H et al 2019 *Phys. Rev. Lett.* **122** 113602
- [36] Liu J et al 2019 *Nat. Nanotechnol.* **14** 586
- [37] Li J-P et al 2021 *Phys. Rev. Lett.* **126** 140501
- [38] Fattal D, Inoue K, Vučković J, Santori C, Solomon G S and Yamamoto Y 2004 *Phys. Rev. Lett.* **92** 037903
- [39] He Y-M, He Y, Wei Y-J, Wu D, Atatüre M, Schneider C, Höfiling S, Kamp M, Lu C-Y and Pan J-W 2013 *Nat. Nanotechnol.* **8** 213
- [40] Ollivier H et al 2021 *Phys. Rev. Lett.* **126** 063602
- [41] Clauser J F, Horne M A, Shimony A and Holt R A 1969 *Phys. Rev. Lett.* **23** 880
- [42] Somaschi N et al 2016 *Nat. Photon.* **10** 340
- [43] Thomas S et al 2021 *Phys. Rev. Lett.* **126** 233601
- [44] Loredó J et al 2019 *Nat. Photon.* **13** 803
- [45] Münzberg J, Draxl F, da Silva S F C, Karli Y, Manna S, Rastelli A, Weihs G and Keil R 2022 *APL Photonics* **7** 070802
- [46] Poderini D, Rodari G, Moreno G, Polino E, Nery R, Suprano A, Duarte C, Sciarrino F and Chaves R 2023 *Phys. Rev. A* **108** 032201
- [47] Agresti I, Poderini D, Carvacho G, Sarra L, Chaves R, Buscemi F, Dall'Arno M and Sciarrino F 2019 *Quantum Sci. Technol.* **4** 035004
- [48] Esposito C, Barros M R, Durán Hernández A, Carvacho G, Di Colandrea F, Barboza R, Cardano F, Spagnolo N, Marrucci L and Sciarrino F 2022 *npj Quantum Inf.* **8** 34
- [49] Tichy M C 2014 *J. Phys. B: At. Mol. Opt. Phys.* **47** 103001
- [50] Zhong H-S et al 2018 *Phys. Rev. Lett.* **121** 250505
- [51] Shahandeh F, Lund A P and Ralph T C 2017 *Phys. Rev. Lett.* **119** 120502
- [52] Carvacho G, Graffitti F, D'Ambrosio V, Hiesmayr B C and Sciarrino F 2017 *Sci. Rep.* **7** 13265
- [53] Karimi E, Leach J, Slussarenko S, Piccirillo B, Marrucci L, Chen L, She W, Franke-Arnold S, Padgett M J and Santamato E 2010 *Phys. Rev. A* **82** 022115